A Rare Case of Kimura's Disease Involving the Parotid Gland: CT and Diffusion MRI

Pasquale Frisina[1]*, Valeria Panebianco[1], Filippo Valentini[2], Alessandro Corsi[1], Daniela Messineo[1]

[1]*Department of Radiological, Oncological and Anatomo-Pathological Sciences, Sapienza University of Rome, Rome, Italy*

[2]*Department of Sense Organs, Sapienza University of Rome, Rome, Italy*

***Correspondence:** Pasquale Frisina, MD, Department of Radiological, Oncological and Anatomo-Pathological Sciences, Sapienza University of Rome, Viale Regina Elena 324, 00161 Rome, Italy

pasquale.frisina@uniroma1.it

Radiology Case. 2026 July; 20(7):1-9 :: DOI: 10.3941/jrcr.6153

AUTHORS' CONTRIBUTIONS

Pasquale Frisina contributed to study conception and design, image analysis, manuscript drafting, and final approval of the submitted version.
Valeria Panebianco contributed to image interpretation, critical revision of the manuscript, and final approval.
Filippo Valentini contributed to clinical data collection, clinicopathological correlation, and manuscript revision.
Alessandro Corsi contributed to histopathological analysis, interpretation of pathological findings, and critical revision of the manuscript.
Daniela Messineo contributed to study supervision, critical revision of the manuscript for important intellectual content, and final approval.

ACKNOWLEDGEMENTS

None

DISCLOSURES

The authors declare no conflicts of interest.

CONSENT

Written informed consent was obtained from the patient for publication of this case report and accompanying images.

HUMAN AND ANIMAL RIGHTS

This article does not contain any studies with human participants or animals performed by any of the authors.

ABSTRACT

Kimura's disease is a rare chronic inflammatory disorder that may involve the parotid gland and closely mimic neoplastic or lymphoproliferative conditions on imaging. We describe the case of a 47-year-old man with parotid gland involvement, evaluated using computed tomography and multiparametric magnetic resonance imaging, with emphasis on diffusion-weighted imaging and quantitative apparent diffusion coefficient analysis.Computed tomography demonstrated a poorly defined soft-tissue mass within the parotid region, associated with intraparotid and cervical lymphadenopathy and heterogeneous contrast enhancement. Magnetic resonance imaging revealed heterogeneous signal intensity, including relatively low T2 signal, and early and progressive, relatively homogeneous enhancement suggestive of an inflammatory process.Quantitative diffusion analysis showed intermediate apparent diffusion coefficient values, consistent with inflammatory tissue rather than highly cellular malignant lesions. Histogram analysis showed a moderately asymmetric distribution, supporting a heterogeneous but non-neoplastic microstructural composition. These findings differed from the typical diffusion patterns of lymphoma and pleomorphic adenoma, with only partial overlap with ductal carcinoma. This case highlights the complementary role of computed tomography and multiparametric magnetic resonance imaging, particularly diffusion-weighted imaging with quantitative apparent diffusion coefficient assessment, in the noninvasive differential diagnosis of rare inflammatory diseases affecting the parotid gland.

CASE REPORT

BACKGROUND

Kimura's disease is a rare chronic inflammatory disorder of unknown etiology, most commonly affecting young to middle-aged men and predominantly reported in Asian populations [1]. Clinically, it presents as painless, slowly enlarging subcutaneous masses, most frequently involving the head and neck region and often associated with regional lymphadenopathy, peripheral eosinophilia, and elevated serum IgE levels. Involvement of the major salivary glands, particularly the parotid gland, is uncommon and represents a diagnostic challenge because this location is more typically associated with benign and malignant salivary gland tumors.

From a radiological perspective, Kimura's disease lacks pathognomonic imaging features and may closely mimic neoplastic or lymphoproliferative disorders [2,3]. Computed

tomography (CT) usually demonstrates ill-defined or infiltrative soft-tissue masses with variable contrast enhancement and frequent association with cervical lymphadenopathy. Magnetic resonance imaging (MRI) typically shows hypointense signal on T1-weighted sequences and variable signal intensity on T2-weighted images, reflecting differing proportions of fibrosis, inflammatory infiltrate, and vascular components. These imaging characteristics substantially overlap with those of malignant parotid tumors and lymphomas, often necessitating histopathological confirmation.

The key epidemiological, clinical, and imaging features of Kimura's disease are summarized in (Table 1).

Diffusion-weighted imaging (DWI) and apparent diffusion coefficient (ADC) analysis provide additional noninvasive information regarding tissue microstructure and cellularity and are increasingly incorporated into the evaluation of parotid gland lesions [4]. Highly cellular malignant tumors generally demonstrate marked diffusion restriction, whereas inflammatory lesions tend to show intermediate diffusion characteristics. However, quantitative diffusion data for Kimura's disease involving the parotid gland remain limited due to the rarity of this entity. In this context, individual case reports supported by multiparametric imaging, including diffusion MRI, may offer valuable insights for improving noninvasive differential diagnosis and guiding clinical management.

CASE REPORT

Clinical Presentation

A 47-year-old man presented with a painless, slowly enlarging mass in the right parotid region. The patient denied fever, weight loss, night sweats, or other systemic symptoms. Physical examination revealed a solid, mobile, non-tender swelling involving both the superficial and deep lobes of the right parotid gland, without facial nerve dysfunction or overlying skin changes. Laboratory evaluation demonstrated marked peripheral eosinophilia (absolute eosinophil count: 2.90 × 10^9/L) and markedly elevated serum IgE levels (28,222 IU/mL; reference range <100 IU/mL).

Imaging Findings

CT demonstrated a large, poorly defined, heterogeneously attenuating soft-tissue mass involving the superficial lobe of the right parotid gland, measuring approximately 9 × 5 × 6 cm. The lesion appeared relatively homogeneous and hypodense on unenhanced images (Figure 1a) and showed heterogeneous enhancement after contrast administration (Figures 1b,1c).

The lesion showed infiltrative growth, extending laterally into the platysma muscle up to the subcutaneous plane, while medially and posteriorly it was inseparable from the sternocleidomastoid muscle and mastoid region. Superiorly, the lesion reached the floor of the external auditory canal, and anteriorly it was partially demarcated from the mandibular ramus and condyle.

An additional smaller lesion with similar attenuation characteristics was identified in the left retromaxillozygomatic space, measuring approximately 25 × 8 mm, suggestive of multifocal involvement.

Multiple intraparotid and right-sided cervical lymph nodes were present at levels IIa–b, III, IV, and Vb, with the largest node measuring 14 mm in short-axis diameter (Figure 1c). Additional subcentimetric lymph nodes were observed at levels IIa–b on the left.

Subsequent multiparametric magnetic resonance imaging (MRI) confirmed the presence of a subcutaneous periauricular lesion extending into the posterior portion of the right parotid gland (Figure 2). On axial T1-weighted images, the lesion demonstrated slightly increased signal intensity relative to muscle, with heterogeneous internal signal and poorly defined margins (Figure 2a). Multiple intraparotid lymph nodes were present and appeared hypointense compared with the surrounding parotid parenchyma. T2-weighted images revealed heterogeneous hyperintensity of the lesion and multiple enlarged intraparotid and lateral cervical lymph nodes, predominantly at levels IIa, III, and Va, with the largest node measuring 14 mm in short-axis diameter (Figure 2b).

Dynamic contrast-enhanced fat-suppressed T1-weighted sequences (VIBE) demonstrated early and progressive enhancement of the lesion, while the intraparotid lymph nodes showed early enhancement with minimal washout, a pattern suggestive of inflammatory and hypervascular tissue (Figure 2c). Axial fat-suppressed T1-weighted spin-echo images confirmed relatively homogeneous enhancement of the lesion and lymph nodes (Figure 2d).

Diffusion-weighted imaging (DWI) and apparent diffusion coefficient (ADC) maps were also evaluated. Mean ADC values were measured on the clinical workstation using region-of-interest analysis on ADC maps, yielding a mean ADC value of 0.80 × 10^{-3} mm²/s, consistent with intermediate diffusion restriction. These findings supported an inflammatory process rather than a highly cellular neoplastic lesion.

Management and Follow-up

Despite the imaging findings and laboratory profile suggestive of an inflammatory etiology, a neoplastic or lymphoproliferative process could not be definitively excluded. The patient therefore underwent radical parotidectomy. Gross pathological examination revealed a solid, well-circumscribed mass involving both the superficial and deep lobes of the parotid gland. Histopathological analysis demonstrated hyperplastic lymphoid follicles with prominent mantle zones (Figure 3a), florid vascular proliferation with abundant eosinophilic infiltration in the interfollicular areas (Figure 3b), and focal areas of sclerosis (Figure 3c). Eosinophilic microabscesses and proteinaceous material within the germinal centers were also observed. Immunohistochemical staining showed IgE positivity within the germinal centers (Figure 3d). These findings were consistent with a diagnosis of Kimura's disease.

DISCUSSION

Etiology & Demographics

Kimura's disease is a rare chronic inflammatory disorder whose imaging appearance frequently overlaps with that of neoplastic and lymphoproliferative diseases, making noninvasive diagnosis particularly challenging. When the parotid gland is involved, this diagnostic difficulty is further amplified, as the majority of parotid masses encountered in clinical practice are benign or malignant salivary gland tumors rather than inflammatory entities. As a result, Kimura's disease is often not initially considered in the differential diagnosis based on imaging findings alone.

Clinical & Imaging Findings

Computed tomography (CT) typically demonstrates nonspecific features in Kimura's disease, including ill-defined or infiltrative soft-tissue masses with variable contrast enhancement and associated cervical lymphadenopathy.

Ultrasound is generally considered the first-line imaging modality for evaluating superficial salivary gland lesions, including the parotid gland, due to its accessibility and ability to assess vascularity. In Kimura's disease, it may demonstrate a hypoechoic or heterogeneous hypervascular mass associated with reactive lymphadenopathy. In the appropriate clinical context, particularly in the presence of peripheral eosinophilia and elevated serum IgE levels, ultrasound can also guide fine-needle aspiration or core needle biopsy as an initial diagnostic step. In this context, cross-sectional imaging is typically performed when deeper extension, multifocality, or diagnostic uncertainty is suspected.

However, CT and MRI provide a more comprehensive assessment of lesion extent, deep tissue involvement, and multifocality. On MRI, lesions are usually hypointense on T1-weighted images and show variable, often heterogeneous hyperintensity on T2-weighted sequences, reflecting different degrees of fibrosis and inflammatory infiltration. After contrast administration, lesions commonly demonstrate moderate to marked enhancement, which may be homogeneous or progressive, and may show internal flow voids related to increased vascularity. Diffusion-weighted imaging typically reveals intermediate diffusion restriction with corresponding ADC values, reflecting the mixed inflammatory and fibrotic composition of the lesion rather than high cellularity.

Dynamic contrast-enhanced MRI has been proposed as a potential adjunct for lesion characterization; however, enhancement patterns in Kimura's disease are variable and nonspecific. Gradual and progressive enhancement is commonly observed but may also be encountered in other inflammatory or hypervascular conditions, thereby limiting its diagnostic specificity. Consequently, perfusion characteristics alone are insufficient to confidently distinguish Kimura's disease from malignant or lymphoproliferative entities [5,6].

In contrast, diffusion-weighted imaging (DWI) and quantitative assessment of the apparent diffusion coefficient (ADC) provide additional insight into tissue cellularity and microstructural organization. Highly cellular malignant tumors, particularly lymphoma, typically demonstrate marked diffusion restriction with low ADC values, whereas benign epithelial tumors with myxoid or cystic components, such as pleomorphic adenoma, generally show higher ADC values. Kimura's disease, reflecting its mixed histopathological composition of inflammatory infiltrates, vascular proliferation, and variable fibrosis, is usually associated with intermediate ADC values.

In the present case, the mean ADC value (0.80×10^{-3} mm²/s) was initially obtained from the vendor-provided clinical workstation using region-of-interest (ROI) measurements performed directly on ADC maps. To further characterize intralesional diffusion heterogeneity, a voxel-based ADC intensity histogram analysis was subsequently performed after lesion segmentation using the LIFEx software, applied to the same ADC dataset (Figure 4) [7]. Histogram analysis demonstrated a unimodal distribution without a dominant low-ADC component (Table 2).

Notably, no voxels with very low ADC values ($<0.6 \times 10^{-3}$ mm²/s) were identified, a feature commonly associated with lymphomatous involvement of the parotid gland. The absence of very low ADC values represents an important discriminating feature against lymphoma. The close correspondence between the mean ADC value derived from the clinical workstation and the peak of the voxel-wise ADC intensity distribution obtained with LIFEx supports the numerical consistency of the diffusion measurements. Additionally, the mild rightward skew of the ADC distribution reflects tissue heterogeneity, consistent with inflammatory pathology rather than uniform high cellularity.

Differential Diagnoses

When considered within the spectrum of common parotid gland lesions (Table 3), the imaging findings observed in this case provide useful discriminative features. Lymphoma typically demonstrates marked diffusion restriction with very low ADC values due to its high cellularity, a feature not observed in the present case, where no very low ADC components were identified. In contrast, pleomorphic adenoma generally shows high ADC values related to its myxoid stroma, which was not consistent with the intermediate ADC values measured in this lesion. Salivary duct carcinoma may show partial overlap, as it can present with intermediate ADC values; however, it typically demonstrates more homogeneous diffusion restriction and different enhancement characteristics. In this case, the combination of heterogeneous signal intensity, progressive enhancement, and intermediate ADC values without a dominant low-ADC component supports an inflammatory rather than malignant process [8].

Treatment & Prognosis

Overall, this case illustrates that while CT and conventional MRI remain essential for lesion detection and anatomical

assessment, diffusion-weighted imaging with quantitative ADC analysis plays a central role in the noninvasive characterization of Kimura's disease involving the parotid gland. Although histopathological confirmation remains necessary for definitive diagnosis, diffusion MRI can meaningfully narrow the differential diagnosis and increase diagnostic confidence in patients with rare inflammatory parotid lesions.

TEACHING POINT

Kimura's disease involving the parotid gland may closely mimic neoplastic and lymphoproliferative lesions on conventional CT and MRI. Diffusion-weighted MRI with quantitative apparent diffusion coefficient analysis can aid in differentiation by demonstrating intermediate diffusion restriction typical of inflammatory tissue rather than the marked restriction seen in highly cellular malignancies. Integration of imaging findings with clinical and laboratory data, including eosinophilia and elevated IgE levels, is essential to suggest the diagnosis, avoid misinterpretation as a malignant tumor, and guide appropriate clinical management.

QUESTIONS & ANSWERS

Question 1: Which imaging features are characteristic of Kimura's disease involving the parotid gland as described in this manuscript? (Select all that apply.)

Ill-defined or infiltrative soft-tissue mass with associated cervical lymphadenopathy on CT. (applies)

Marked diffusion restriction with very low ADC values comparable to lymphoma.

Variable signal intensity on T2-weighted MRI reflecting mixed tissue composition. (applies)

Progressive or gradual contrast enhancement on dynamic MRI. (applies)

Predominantly cystic lesion with high ADC values typical of pleomorphic adenoma.

Explanation: The manuscript describes a poorly defined parotid mass with associated intraparotid and cervical lymphadenopathy on CT, as well as heterogeneous MRI signal characteristics. The variable T2-weighted signal reflects differing proportions of inflammation, fibrosis, and vascular components. Dynamic contrast-enhanced MRI demonstrated gradual and progressive enhancement, a pattern more consistent with inflammatory tissue. Marked diffusion restriction with very low ADC values and predominantly cystic features were not observed and are more typical of lymphoma and pleomorphic adenoma, respectively.

Question 2: What diffusion-weighted MRI findings supported an inflammatory rather than malignant etiology in this case? (Select all that apply.)

Intermediate apparent diffusion coefficient (ADC) values. (applies)

Absence of a dominant low-ADC peak on histogram analysis. (applies)

Uniform and marked diffusion restriction throughout the lesion.

ADC values consistent with highly cellular malignancies.

Heterogeneous diffusion profile reflecting mixed tissue composition. (applies)

Explanation: Quantitative diffusion analysis revealed intermediate ADC values, consistent with inflammatory tissue rather than highly cellular malignancies. Histogram analysis showed a moderately asymmetric distribution without a dominant low-ADC peak, supporting a heterogeneous microstructural composition. Uniform and marked diffusion restriction is typical of lymphoma and was not observed in this case.

Question 3: Which laboratory and clinical findings supported the diagnosis of Kimura's disease in this patient? (Select all that apply.)

Marked peripheral eosinophilia. (applies)

Elevated serum IgE levels. (applies)

Rapidly progressive painful parotid swelling with fever.

Painless, slowly enlarging parotid mass. (applies)

Early facial nerve palsy.

Explanation: The patient presented with a painless, slowly enlarging parotid mass and showed marked peripheral eosinophilia and significantly elevated serum IgE levels, which are characteristic features of Kimura's disease. Systemic symptoms such as fever, rapid progression, or facial nerve palsy were not present and would be more suggestive of infectious or malignant conditions.

Question 4: Which histopathological findings are consistent with Kimura's disease as described in this manuscript? (Select all that apply.)

Hyperplastic lymphoid follicles with prominent mantle zones. (applies)

Florid vascular proliferation with eosinophilic infiltration. (applies)

Extensive tumor necrosis and high mitotic activity.

Eosinophilic microabscesses and sclerosis. (applies)

IgE positivity within germinal centers on immunohistochemistry. (applies)

Explanation: Histopathological examination revealed hyperplastic lymphoid follicles, florid vascular proliferation, abundant eosinophils, areas of sclerosis, and eosinophilic microabscesses. Immunohistochemical staining demonstrated IgE positivity within germinal centers. Features such as extensive necrosis and high mitotic activity were not present and would favor malignant pathology.

Question 5: When considering the differential diagnosis of parotid gland lesions, which statements regarding Kimura's disease are supported by the manuscript? (Select all that apply.)

Kimura's disease may closely mimic malignant salivary gland tumors on conventional imaging. (applies)

Lymphoma typically shows lower ADC values than Kimura's disease. (applies)

Pleomorphic adenoma generally demonstrates higher ADC values than Kimura's disease. (applies)

Diffusion MRI alone is sufficient for definitive diagnosis without histology.

Integration of imaging findings with clinical and laboratory data improves diagnostic confidence. (applies)

Explanation: The manuscript emphasizes that Kimura's disease can closely mimic neoplastic and lymphoproliferative lesions on CT and conventional MRI. Lymphoma typically exhibits lower ADC values, while pleomorphic adenoma shows higher ADC values due to myxoid components. Although diffusion MRI provides valuable diagnostic information, histopathological confirmation remains necessary, and integration of imaging, clinical, and laboratory findings is essential.

REFERENCES

[1] Zhang R, Ban X, Mo Y, et al. Kimura's disease: the CT and MRI characteristics in fifteen cases. *Eur J Radiol*. 2011; 80(2): 489–497. PMID: 21030173.

[2] Horikoshi T, Motoori K, Ueda T, et al. Head and neck MRI of Kimura disease. *Br J Radiol*. 2011; 84(1005): 800–804. PMID: 21849365.

[3] Park SW, Kim HJ, Sung MS, et al. Kimura disease: CT and MR imaging findings. *AJNR Am J Neuroradiol*. 2012; 33(4): 784–788.

[4] Sangwan A, Goyal A, Bhalla AS, et al. Kimura disease: a case series and systematic review of clinico-radiological features. *Curr Probl Diagn Radiol.* 2022; 51(1): 130–142. PMID: 33250297.

[5] Gökçe E. Multiparametric magnetic resonance imaging for the diagnosis and differential diagnosis of parotid gland tumors. *J Magn Reson Imaging.* 2020; 52(1): 11-32. PMID: 32065489.

[6] Pietragalla M, Nardi C, Bonasera L, et al. The role of diffusion-weighted and dynamic contrast-enhanced perfusion-weighted imaging in the evaluation of salivary gland neoplasms. *Radiol Med.* 2020; 125(9): 851-863. PMID: 32266692.

[7] Nioche C, Orlhac F, Boughdad S, et al. LIFEx: a freeware for radiomic feature calculation in multimodality imaging to accelerate advances in the characterization of tumor heterogeneity. *Cancer Res.* 2018; 78(16): 4786–4789. PMID: 29959149.

[8] Luo Y, Yang G, Shi H, et al. A stepwise decision-tree model for differential diagnosis of Kimura's disease in the head and neck. *BMC Med Imaging.* 2025; 25: 90.

FIGURES

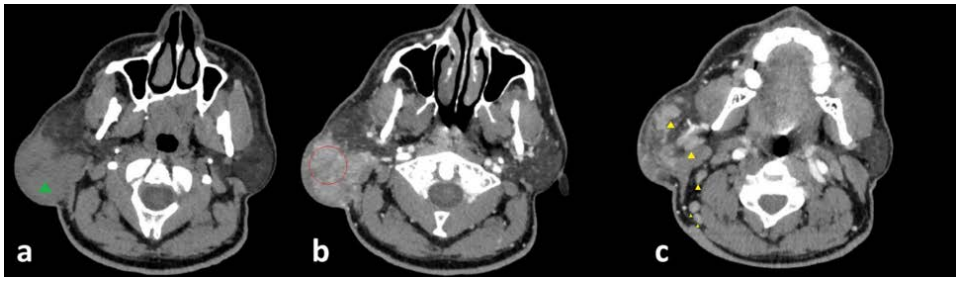

Figure 1: A 47-year-old man with a painless, slowly enlarging mass in the right parotid region. Kimura's disease.(a) Axial unenhanced CT image demonstrating a soft-tissue lesion in the right parotid region (green triangle).(b) Axial contrast-enhanced CT image acquired in the venous phase after intravenous administration of iodinated contrast medium, showing a relatively well-defined enhancing mass involving the right parotid gland (red circle).(c) Axial contrast-enhanced CT image demonstrating associated lateral cervical lymphadenopathy (yellow triangles).

Axial multislice computed tomography of the neck performed before and after intravenous administration of iodinated contrast material, with images acquired in the venous phase.

Technique: Contrast-enhanced multislice computed tomography (CT) of the neck was performed using a volumetric acquisition before and after intravenous administration of nonionic iodinated contrast material (iopromide, Ultravist 370 mgI/mL; 80 mL at 3 mL/s).

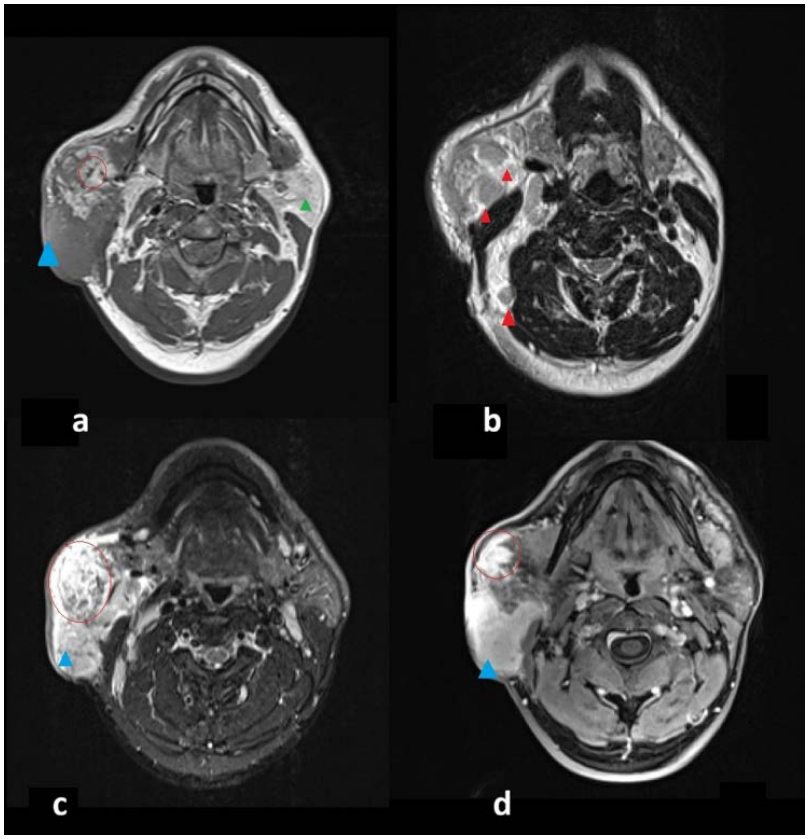

Figure 2: A 47-year-old man with a painless, slowly enlarging mass in the right parotid region. Kimura's disease. Multiparametric MRI of the neck. (a) Axial T1-weighted image demonstrates a subcutaneous periauricular lesion (blue triangle) with slightly increased signal intensity relative to adjacent muscle and poorly defined margins. An intraparotid lymph node (red circle) shows lower signal intensity relative to the surrounding parotid parenchyma (green triangle). (b) Axial T2-weighted image shows a heterogeneous signal intensity, including relatively low T2 signal, associated with intraparotid and lateral cervical lymphadenopathies (red triangles). (c) Axial dynamic contrast-enhanced fat-suppressed T1-weighted gradient-echo image (VIBE) demonstrates early and progressive enhancement of the lesion (blue triangle), without significant washout, consistent with an inflammatory pattern, and showing subtle internal signal voids suggesting vascularity. The intraparotid lymph node (red circle) shows early enhancement.. (d). Axial fat-suppressed T1-weighted spin-echo image shows relatively homogeneous enhancement of the lesion (blue triangle). The intraparotid lymph node (red circle) also demonstrates homogeneous enhancement.

Technique: MRI was performed on a 1.5-T scanner using two-dimensional axial T1-weighted spin-echo sequences (slice thickness 3 mm), high-resolution T2-weighted turbo spin-echo sequences, dynamic contrast-enhanced fat-suppressed T1-weighted sequences (VIBE), and fat-suppressed T1-weighted spin-echo sequences after intravenous administration of gadoteridol (ProHance®, 16 mL; injection rate 2.0 mL/s).

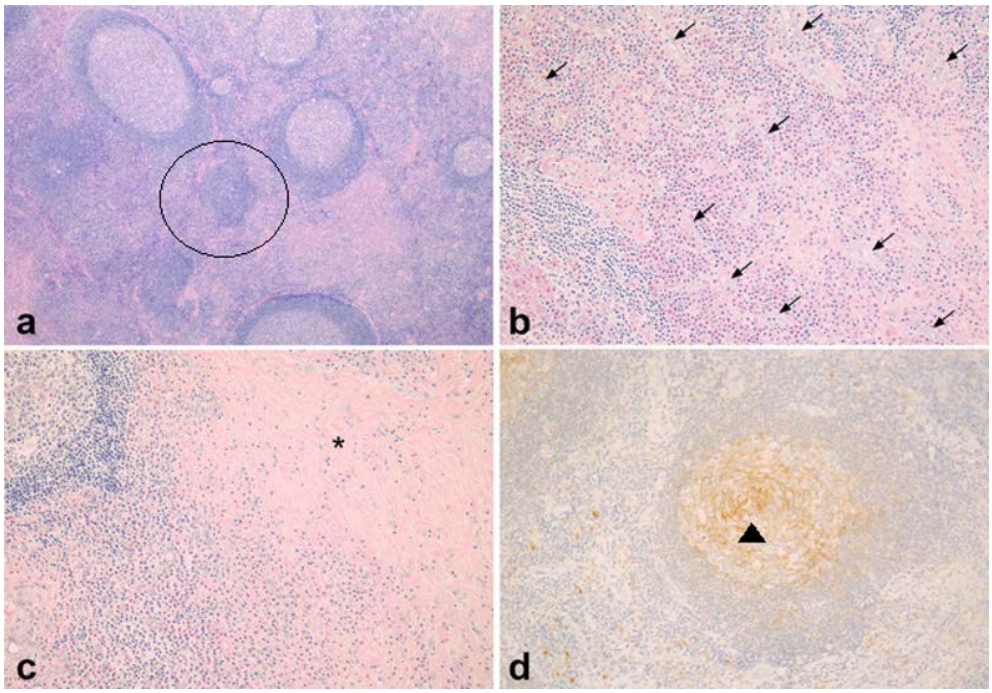

Figure 3: A 47-year-old man with a painless, slowly enlarging mass in the right parotid region. Kimura's disease.(a) Hyperplastic lymphoid follicles and expansion of the interfollicular areas (circle). (b) Florid vascular proliferation (arrows) with abundant eosinophilic granulocytes in the interfollicular area. (c) Areas of sclerosis within the interfollicular region (asterisk). (d) Immunohistochemical staining demonstrating IgE positivity within a germinal center (brown color, triangle).Histopathological examination of parotid gland tissue. Panels a–c: hematoxylin–eosin staining; panel d: immunohistochemistry for IgE. Original magnification: 4× for panel a and 10× for panels b–d. Scale bars: 200 µm in panel a and 100 µm in panels b–d.

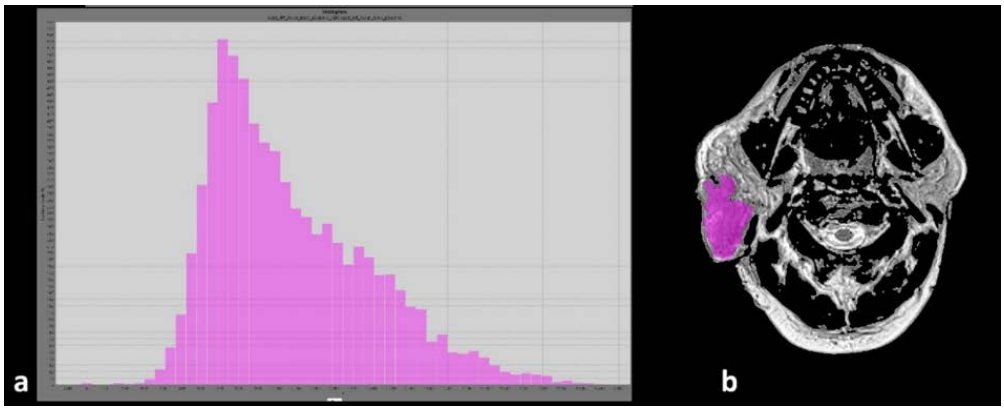

Figure 4: A 47-year-old man with a painless, slowly enlarging mass in the right parotid region. Kimura's disease. (a) Histogram of apparent diffusion coefficient (ADC) values per voxel within the region of interest (ROI), derived from diffusion-weighted imaging, demonstrating a unimodal distribution without a dominant low-ADC component.(b) Corresponding axial ADC map showing the segmented lesion (ROI). Diffusion-weighted magnetic resonance imaging of the neck with ADC map reconstruction; voxel-based ADC histogram analysis performed after ROI segmentation using LIFEx software.

Table 1: Summary of epidemiological, clinical, and imaging characteristics of Kimura's disease.

Parameter	Description
Etiology	Chronic immune-mediated inflammatory disorder; Th2-driven hypersensitivity with eosinophilia and elevated IgE
Incidence	Rare; <1 per 100,000 individuals
Gender ratio	Male predominance (approximately 3–5:1)
Age predilection	Young to middle-aged adults; most commonly 20–50 years
Risk factors	Atopy, allergic predisposition, elevated serum IgE
Treatment	Surgical excision, corticosteroids, immunosuppressive therapy; radiotherapy in refractory cases
Prognosis	Benign but chronic course; frequent local recurrence
Findings on imaging	Ill-defined enhancing soft-tissue mass with lymphadenopathy; intermediate ADC values on DWI

Table 2: Voxel-based apparent diffusion coefficient (ADC) intensity histogram characteristics derived from LIFEx software analysis in the present case.

Parameter	Value
ADC unit	$\times 10^{-3}$ mm²/s
ADC range observed on histogram	0.0 – 2.8
Lower bound of predominant distribution	0.6
Upper bound of predominant distribution	1.2
Peak ADC value (histogram mode)	0.8
Histogram modality	Unimodal
Distribution skewness	Right-skewed
Presence of very low ADC values (<0.6 $\times 10^{-3}$ mm²/s)	Absent
Presence of high ADC tail (>1.8 $\times 10^{-3}$ mm²/s)	Present
Overall diffusion pattern	Intermediate diffusion restriction consistent with heterogeneous inflammatory tissue

Table 3: Comparison of apparent diffusion coefficient (ADC) values among Kimura's disease and common parotid gland lesions.

Lesion	Mean ADC value / range ($\times 10^{-3}$ mm²/s)	Interpretation
Kimura's disease (present case)	0.80	Intermediate diffusion restriction
Kimura's disease (literature)	0.7 – 1.1	Intermediate diffusion restriction
Lymphoma	0.4 – 0.7	Marked diffusion restriction
Salivary duct carcinoma	0.8 – 1.2	Intermediate, relatively uniform restriction
Warthin tumor	0.6 – 1.0	Variable, often relatively low ADC
Pleomorphic adenoma	1.4 – 2.2	High ADC values

KEYWORDS

Kimura's disease; Parotid gland; Computed tomography; Head and neck MRI; Diffusion-weighted imaging;

ABBREVIATIONS

ADC = Apparent Diffusion Coefficient
KD = Kimura's Disease
LIM = Lymphoma
PL = Pleomorphic Adenoma
DC = Ductal Carcinoma
WT = Warthin Tumor
MRI = Magnetic Resonance Imaging
CT = Computed Tomography
ROI = Region Of Interest
T2-w = T2-Weighted
MP-MRI = Multi Parametric Magnetic Resonance Imaging